Journal of Solid State Chemistry **163,** 231–238 (2002)
doi:10.1006/jssc.2001.9397, available online at http://www.idealibrary.com on IDEAL®

Effects of Metal Ion Sources on Synthesis and Electrochemical Performance of Spinel $LiMn_2O_4$ Using Tartaric Acid Gel Process

Y. M. Hon, K. Z. Fung,[1] S. P. Lin, and M. H. Hon

Department of Materials Science and Engineering, National Cheng Kung University, Tainan 70101, Taiwan

Received June 8, 2001; in revised form September 5, 2001; accepted September 14, 2001; published online November 27, 2001

The effect of lithium and manganese ions on the synthesis, phase purity, and electrochemical properties of tartaric acid gel processed lithium manganese oxide spinel were investigated. The poor bonding between both lithium and manganese ions with tartaric acid was shown by the FT-IR analysis when lithium nitrate and/or manganese nitrate were used as sources. Li_2MnO_3 and Mn_2O_3 impurities formed in addition to lithium manganese oxides when nitrate salts were used as the sources. When acetate salts were used as sources for the lithium and manganese ions, single-phase $LiMn_2O_4$ was obtained. These results indicate that homogeneous bonding between acetate salt and tartaric acid was formed. The capacity of single-phase $LiMn_2O_4$ calcined at 500°C was 117 mAh/g which was much higher than those containing Mn_2O_3 and Li_2MnO_3 impurity compounds. Thus, sources of lithium and manganese ions play an important role in the synthesis and electrochemical behaviors of lithium manganese oxide spinel.

Key Words: **$LiMn_2O_4$; tartaric acid; nitrate salts; acetate salts; cathode; lithium-ion battery.**

1. INTRODUCTION

The high-energy density lithium-ion battery was used widely in portable electronic products, such as cellular phone, notebook, and video camera, etc. (1–3). The lithium-ion battery using $LiMn_2O_4$ as the cathodic electrode has shown several advantages over $LiCoO_2$ and $LiNiO_2$, such as (1) lower cost resulting from abundant resources and (2) lower toxicity compared to Co and Ni (4–6).

Transition metal oxide powders are usually fabricated by the conventional solid-state reaction method which requires a higher calcination temperature followed by several grinding and annealing processes that are not suitable for better control of particle size distribution. Generally, as for the battery application, it is believed that single-phase, homogeneity, uniform particle morphology with submicrometer size distribution, and high surface area are desired features in order to achieve a higher electrode activity (7). In recent years, "soft-chemical" method was widely used to synthesize the desired powders, such as sol-gel (8, 9), melt-impregnation (10), tartaric acid/citric acid gel process (11–13), Pechini process (14, 15), and solution-based oxidation method (16) which mainly focused on developing techniques for preparing stoichiometric and single-phase ultrafine powders.

The effects of starting materials and the synthesis temperature on specific surface area and electrochemical properties of $LiMn_2O_4$ powders by solid-state reaction method had been studied by Momchilov (17). Barboux (18) investigated the roles of starting materials and ambient atmosphere on the synthesis of $Li_xMn_2O_4$ phase by coprecipitation method. The effects of Li/Mn ratio and atmosphere on synthesis mechanism and electrochemical properties of $Li_xMn_2O_4$ were emphasized.

In our previous studies (11, 19), the tartaric acid gel process has been developed to fabricate nano-$LiMn_2O_4$ powder because this process provides several advantages of (i) high specific surface area, (ii) better control in the ratio of lithium to manganese, and (iii) easily accessible procedures.

In this work, the effects of lithium manganese tartrate precursors prepared from different lithium and manganese salts on synthesis, phase purity, and electrochemical properties of $LiMn_2O_4$ powders were investigated.

2. EXPERIMENTAL PROCEDURE

Lithium acetate (98% purity, Aldrich), lithium nitrate (99% purity, Acros Organics), manganese acetate (99% purity, Showa Chemicals Inc.), and manganese nitrate (98.5% purity, Merck), respectively, were used as sources of lithium and manganese ions in this study. Since nitrate salts are hygroscopic, a dry box was used to store and process nitrate salts. The lithium and manganese salts with a cationic ratio of Li : Mn = 1 : 2 were dissolved in ethanol and mixed well with an ethanol solution of tartaric acid (99.5% purity, Katayama), which was used as chelating agent. The molar ratio of tartaric acid to total metal ions

[1] To whom correspondence should be addressed. Fax: 886-6-2380208. E-mail: kzfung@mail.ncku.edu.tw.

0022-4596/02 $35.00

was set at 1:0.75. During mixing, the solution abruptly transformed into a viscous gel. The final gel contained 0.025 M Li^+, 0.05 M Mn^{2+}, and 0.1 M tartaric acid. The resulting solution was dried at 68°C and subsequently calcined at 265 to 800°C for 24 h in air.

Thermal analysis was conducted to examine the heat and weight changes during the calcination process. Thermal analysis was carried out using differential scanning calorimeter (DSC, Netzsch 404) and thermogravimetric analysis (TG, TA2950) to investigate the possible phase transformations between 25 and 500°C at a heating rate of 5°C/min in air. Fourier transform infrared spectrometer (FT-IR, Jasco FT/IR-410) was used to study the structure coordination of the precursors. Each sample was mixed with KBr and examined at the wavenumber range from 1000 to 4000 cm^{-1}. The phase identity of samples was investigated using Rigaku X-ray diffractometer (XRD) with the Cu$K\alpha$ radiation at 30 kV, 20 mA. The XRD data were collected between 10° and 70° of 2θ angles with a step interval of 0.01° and a scanning rate of 1°/min.

To determine the chemical composition, Li and Mn concentration of single-phase $LiMn_2O_4$ were measured by inductively coupled plasma (ICP, Janell-Ash, ICAP 9000). The average valence of manganese in single-phase $LiMn_2O_4$ was determined by the titration method. About 0.06 g of the sample was dissolved in 20 ml of an acidified 0.08 M Fe(II) solution. During dissolution, the higher Mn oxidation states (III) and (IV) were reduced to Mn(II) by the oxidation of Fe(II) to Fe(III). The excess Fe(II) was back titrated with 0.018 M $KMnO_4$.

Electrochemical measurements were carried out using coin-type cells (CR2032). The reference and counterelectrodes were constructed from the lithium foil (FMC). The electrolyte was a 1:1 (v/v) mixture of ethylene carbonate (EC) and diethyl carbonate (DEC) containing 1 M $LiPF_6$ (Mitsubishi Chemical). The cathode contained 70% active material, 17% KS-6 carbon black, and 13% polyvinylidene fluoride (PVDF) binder. The cell was assembled in an argon-filled dry box. Charge–discharge cycling tests were performed at current density of 0.1 mA/cm^2 in the voltage range between 3.0 and 4.2 V at 25°C.

3. RESULTS AND DISCUSSION

3.1. Thermal Analysis

Figure 1 shows the TG/DSC curves of lithium manganese tartrate precursors prepared by different sources of lithium and manganese salts. From thermogravimetric analysis, the weight loss of precursors using manganese nitrate as the manganese source is larger than that using manganese acetate salts as the sources when temperature reached 80°C. The DSC traces of precursors prepared from nitrate salts have a small endothermic broadened peak at about 80°C. This endothermic reaction was not observed when the precursor was prepared by lithium acetate and manganese acetate. This result indicates that the reaction at about 80°C is attributed to the decomposition of nitrate groups.

As the temperature increased, an abrupt weight loss occurred at about 350°C accompanied with a sharp exothermic peak, which is due to the combustion of the organic component and formation of lithium manganese oxide (11). At about 350°C, the weight loss of precursor using lithium acetate and manganese acetate as sources is apparently less than those prepared from lithium nitrate and manganese nitrate. The temperature of exothermic reaction from acetate salt is higher than that from nitrate salts. Above 400°C, the changes in TG and DSC curves for all precursors were insignificant, indicating that most of the organic group had been removed.

3.2. Phase Analysis

3.2.1. Precursor Prepared from Various Salts

3.2.1.1. Lithium acetate and manganese acetate. Since the heating rate for TG/DSC was as high as 5°C/min and the final decomposition of precursors ended at 400°C, the reaction should occur at temperatures significantly lower than 400°C. It is believed that lithium manganese oxide can be formed at much lower temperatures. Thus, the precursors were calcined at temperatures as low as 265°C. Figure 2 shows the XRD patterns of powders calcined at various temperatures using lithium acetate and manganese acetate as sources. The lithium manganese oxide spinel formed after calcined at 265°C for 24 h. However, the crystallinity of the powder was poor at this temperature. The diffraction peaks gradually sharpened with increasing annealing temperature, suggesting an increase of crystallinity. When lithium manganese tartrate precursor was calcined at 500 and 600°C, lithium manganese oxide with negligible amount of Mn_2O_3 was obtained. This result suggests that this tartaric acid gel process is much superior to commonly used solid-state reaction for synthesizing lithium manganese oxide powders. The fact that $LiMn_2O_4$ spinel powders can be prepared at a much lower temperature can be attributed to the shorter Li–Mn ion distance and atomic-scale metal ion distribution in the precursor (11).

3.2.1.2. Lithium nitrate and/or manganese nitrate. The XRD patterns of powders calcined at various temperatures using lithium nitrate and/or manganese nitrate are shown in Fig. 3. It was observed that the lithium manganese oxides formed at temperatures lower than 500°C. Above 500°C, impurity phase of Mn_2O_3 and orange powder appeared on the surface of calcined powders. From XRD patterns shown in Fig. 3d, the orange powder was found to be Li_2MnO_3 compound. It has been reported that Mn_2O_3 was also

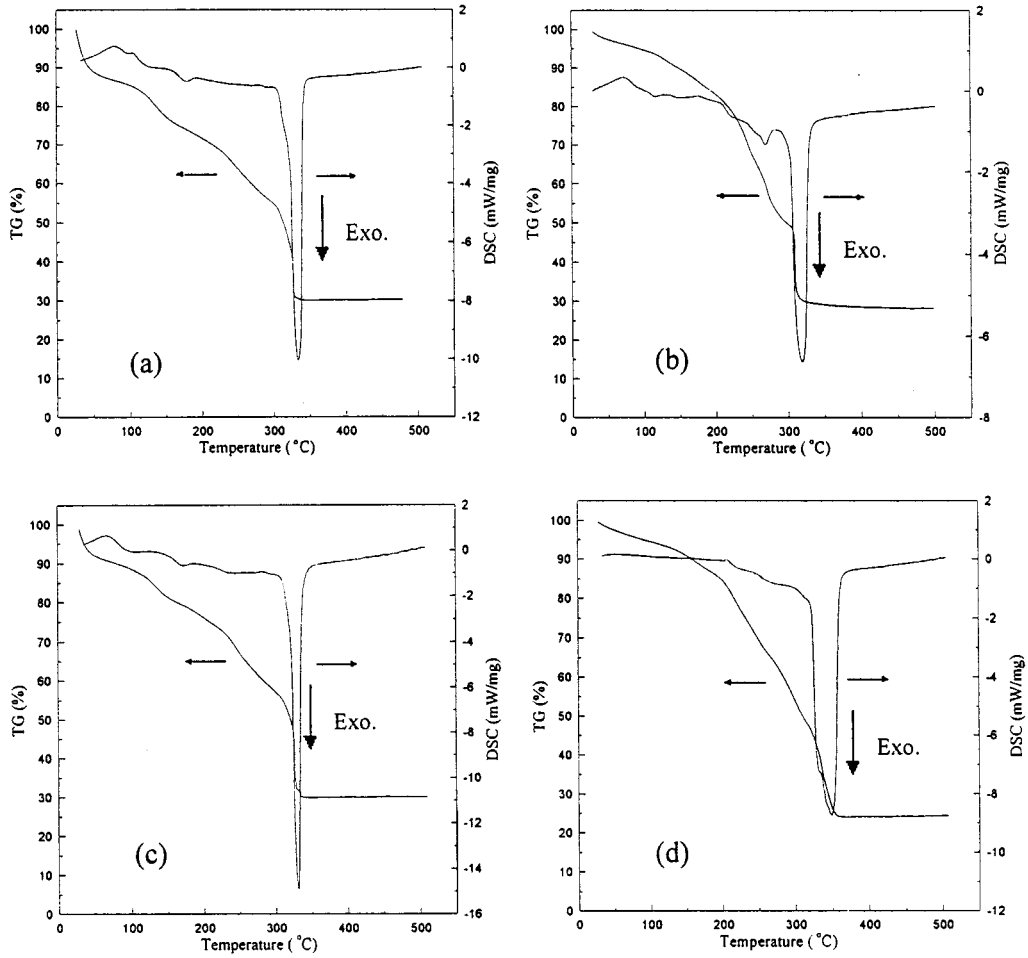

FIG. 1. TG/DSC curves of lithium manganese tartrate precursors using (a) lithium nitrate and manganese nitrate, (b) lithium nitrate and manganese acetate, (c) lithium acetate and manganese nitrate, and (d) lithium acetate and manganese acetate, as sources with a heating rate of 5°C/min.

present when lithium manganese oxide was synthesized at 500°C using solution-based oxidation method (16). However, the amount of Mn_2O_3 decreases as the firing temperature increases. At 800°C, Mn_2O_3 reacted with lithium manganese oxide and was not observed. In Fig. 3, however, Mn_2O_3 was still when the powder was calcined at 800°C. It is believed that the appearance of Li_2MnO_3 hinders the dissolution of Mn_2O_3 into lithium manganese oxide because

(i) Li_2MnO_3 has a NaCl-type structure which is different from spinel structure;

(ii) the precipitation of Li_2MnO_3 depletes Li ions from lithium manganese oxide.

3.3. Effect of Metal Ion Sources on Bonding between Metal Ions and Tartaric Acid

In the present study, it was found that the single-phase $LiMn_2O_4$ spinel was synthesized only when lithium acetate and manganese acetate were used as sources. When lithium nitrate and/or manganese nitrate salts were used as the sources, impurity phases of Mn_2O_3 and Li_2MnO_3 were formed along with lithium manganese oxide spinel. Such a variation may be caused by the different bonding strength of lithium and manganese ions with tartaric acid. Thus the FT-IR was used to analyze the lithium manganese tartrate precursors.

Figure 4 shows the FT-IR spectra of tartaric acid, lithium nitrate–tartrate and lithium acetate–tartrate precursors. For pure tartaric acid, the broad IR band located at 3317 cm^{-1} is attributed to the O–H streching vibration. Also, bands corresponding to carboxylate anion were observed at 1740, 1625, and 1340 cm^{-1}, respectively. For lithium nitrate–tartrate and lithium acetate–tartrate precursors, the difference in O–H stretching vibration from tartaric acid was observed. A new IR band was formed at 3611 cm^{-1}, suggesting the lithium ion from lithium nitrate and acetate salts bonds with the O–H streching vibration.

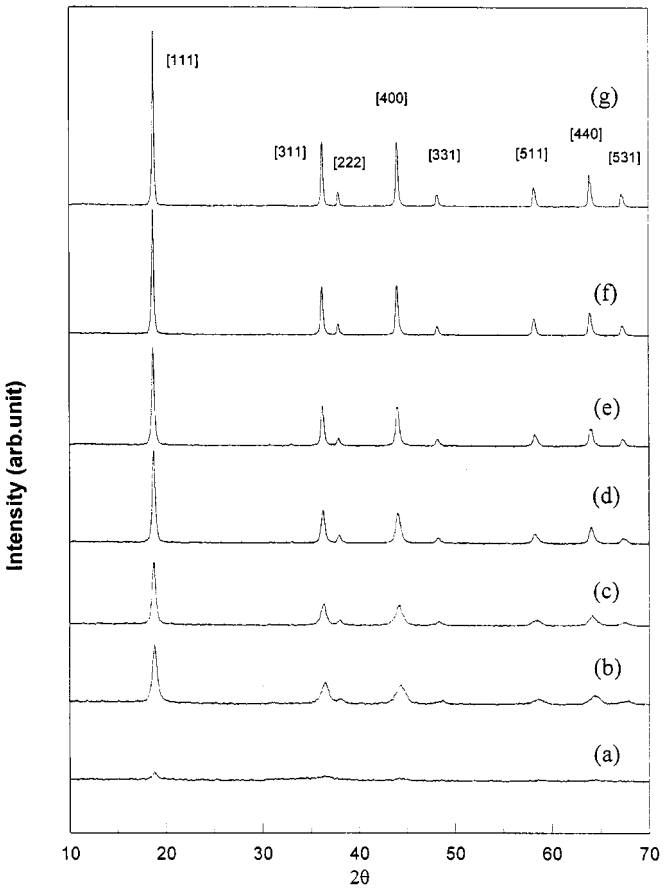

FIG. 2. XRD patterns of powders calcined at (a) 265°C, (b) 300°C, (c) 400°C, (d) 500°C, (e) 600°C, (f) 700°C, and (g) 800°C for 24 h using lithium acetate and manganese acetate as sources.

However, the IR band at 3611 cm^{-1} for lithium nitrate–tartrate precursor is broader and weaker than that for lithium acetate–tartrate precursor. Thus, the bonding strength between lithium ion and O–H stretching is stronger for lithium acetate–tartrate precursor than that for lithium nitrate–tartrate precursor. In addition, bands corresponding to carboxylate anion at 1740, 1625, and 1340 cm^{-1} split into several peaks was found in lithium acetate–tartrate precursor. However, the bands corresponding to carboxylate anion for lithium nitrate–tartrate precursor is almost the same with that of tartaric acid. These results indicate that the lithium ion from lithium acetate salt firmly bonds with O–H stretching and carboxylate anion of tartaric acid. Lithium ion from lithium nitrate salt only bonds with O–H stretching but not with carboxylate anion of tartaric acid.

In regard to manganese ion sources, Fig. 5 shows the FT-IR spectra of tartaric acid, manganese nitrate–tartrate and manganese acetate–tartrate precursors. The broad IR band located at 3317 cm^{-1} of O–H stretching vibration for tartaric acid did not show any changes for either manganese nitrate–tartrate or manganese acetate–tartrate precursors. Bands corresponding to carboxylate anion at 1740, 1625, and 1340 cm^{-1} of tartaric acid varies for both manganese nitrate–tartrate and manganese acetate–tartrate precursors. This result demonstrates the different bonding strength of manganese–carboxylate anion for manganese nitrate–tartrate and for manganese acetate–tartrate precursors.

From the results of FT-IR analysis, the lithium ion from lithium acetate salt formed strong bonding with O–H stretching and carboxylate anion of tartaric acid. However, the lithium ion only bonds with O–H stretching but not with carboxylate anion of tartaric acid when lithium nitrate was used as the source of lithium. The lithium ions that did not bond with tartaric acid apparently segregated on the surface of lithium manganese precursor. Thereafter, Li-rich Li_2MnO_3 was formed on the surface of powder. That is the main reason why single-phase $LiMn_2O_4$ spinel can be synthesized only when lithium and manganese acetate salts are used as the sources.

3.4. Effect of Phase Purity on Electrochemical Properties

Figure 6 shows the first discharge curves of samples calcined at 500°C with cut-off voltage varied from 3.0 to 4.2 V. The discharge curves of all samples exhibit two pseudo plateaus, which is a typical profile for the electrochemical extraction and insertion of lithium ion. This result confirms two equilibrium binary systems during Li^+ intercalation, i.e., λ-MnO_2–$Li_{0.5}Mn_2O_4$ and $Li_{0.5}Mn_2O_4$–$LiMn_2O_4$ (20).

Figure 7 shows the discharge capacity vs cycle number for powders calcined at 500°C using different lithium and manganese salts with cutoff voltage from 3.0 to 4.2 V. The first discharge capacity of single-phase $LiMn_2O_4$ using lithium acetate and manganese acetate as sources delivered 117 mAh/g and remained at 105 mAh/g after 13 cycles. The capacity of synthesized powders using lithium nitrate/manganese nitrate, lithium nitrate/manganese acetate, and lithium acetate/manganese nitrate as sources delivered initial capacities of 75, 81, and 81 mAh/g, respectively, which were only 51 and 55% of the theoretical capacity. From Fig. 2, it was shown that single-phase $LiMn_2O_4$ was obtained only when lithium acetate and manganese acetate were used as ion sources. For samples using nitrate(s) ion source(s), impure phases of Mn_2O_3 and Li_2MnO_3 were found. Both phases are inactive for lithium intercalation reaction. Furthermore, the lithium manganese oxide synthesized from nitrate sources became lithium and manganese-deficient nonstoichiometric spinel. Although the exact amount of Mn_2O_3 and Li_2MnO_3 was difficult to be determined, the nonstoichiometric lithium manganese oxide spinel may be

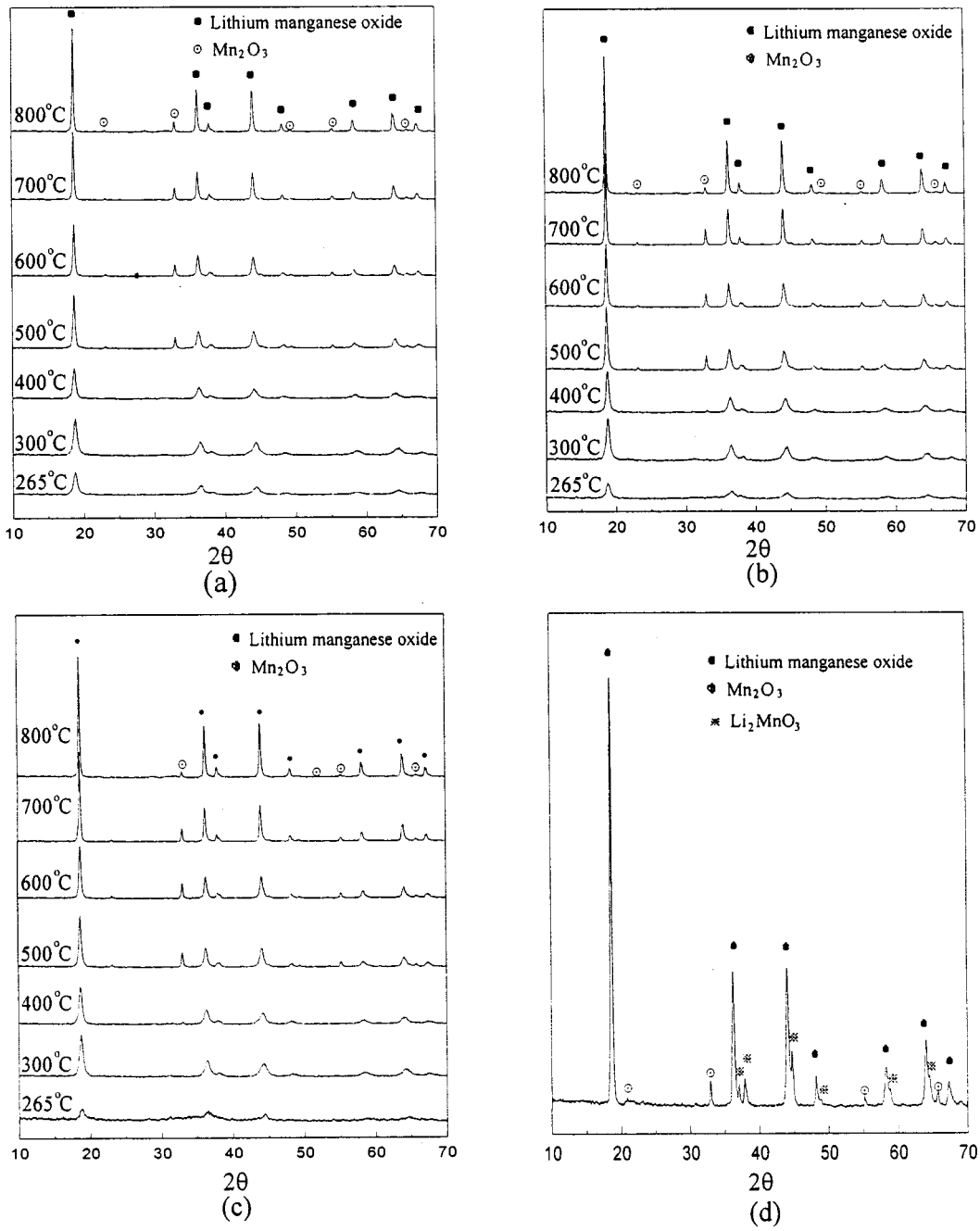

FIG. 3. XRD patterns of powders calcined at various temperatures which (a) lithium nitrate and manganese nitrate, (b) lithium nitrate and manganese acetate, (c) lithium acetate and manganese nitrate, and (d) orange powder on the surface of sample calcined at 800°C using lithium nitrate and manganese nitrate as sources.

described from the following reaction:

$$LiMn_2O_4 \rightarrow Li_{1-2z}Mn_{2-2y-z}O_{4-3y-3z} + yMn_2O_3 + zLi_2MnO_3.$$

Thus, the degradation in capacity for samples using nitrate as ion sources may result from the presence of impure phase and the nonstoichiometry of $Li_{1-2z}Mn_{2-2y-z}O_{4-3y-3z}$ spinel. These results suggest the electrochemical properties of lithium manganese oxide are strongly affected by the different ion sources.

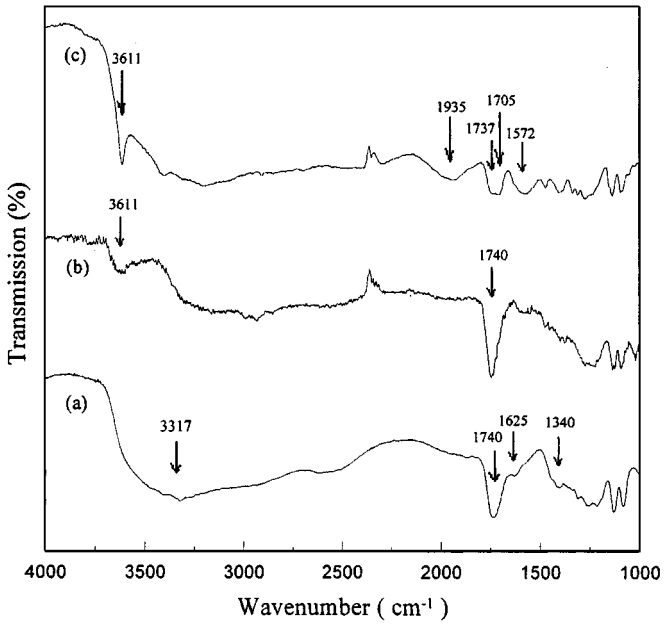

FIG. 4. FT-IR spectra for (a) tartaric acid, (b) lithium nitrate–tartrate, and (c) lithium acetate–tartrate precursors.

3.5. Acetate-Derived Single-Phase Lithium Manganese Oxide

From the result of XRD, the single-phase $LiMn_2O_4$ can be synthesized using acetate salt as the sources. The capacity

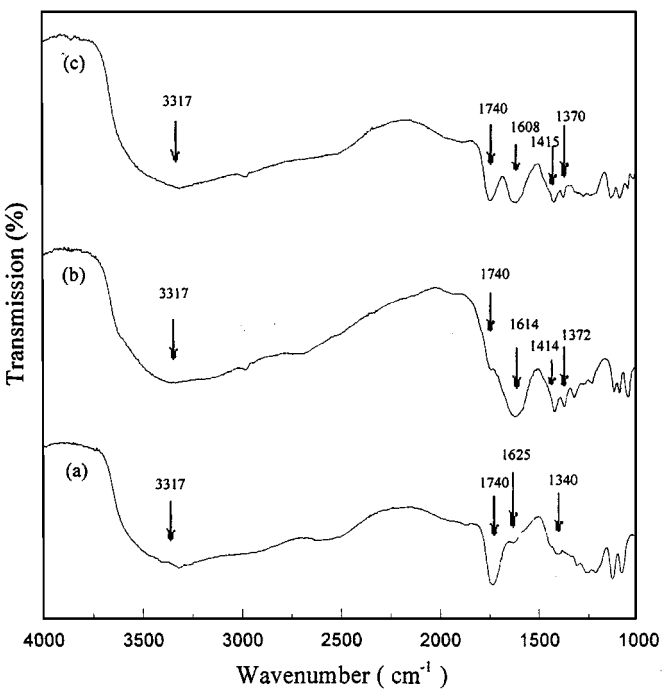

FIG. 5. FT-IR spectra for (a) tartaric acid, (b) manganese nitrate–tartrate, and (c) manganese acetate–tartrate precursors.

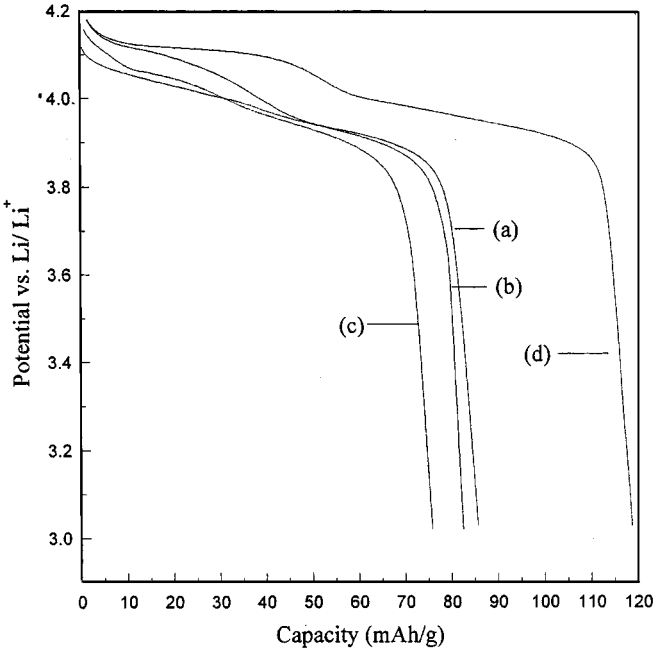

FIG. 6. The first discharge curves of powders calcined at 500°C using (a) lithium nitrate and manganese nitrate, (b) lithium nitrate and manganese acetate, (c) lithium acetate and manganese nitrate, and (d) lithium acetate and manganese acetate as sources.

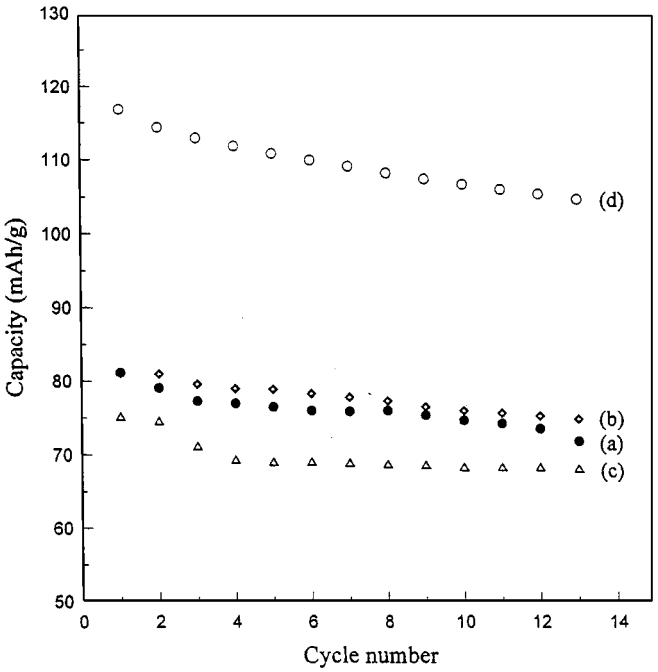

FIG. 7. Discharge capacity vs cyclic number of powders calcined at 500°C using (a) lithium nitrate and manganese nitrate, (b) lithium nitrate and manganese acetate, (c) lithium acetate and manganese nitrate, and (d) lithium acetate and manganese acetate as sources with cutoff voltage of 3.0 to 4.2 V.

TABLE 1
Chemical Analyses and Electrochemical Properties of Lithium Manganese Oxide Spinels Calcined at Various Temperatures

Temperature (°C)	Li (wt%)[a]	Mn (wt%)[a]	Li/Mn ratio	Average valence of Mn[a]	Mn^{3+} (wt%)[b]	Discharge capacity at 1st cycle (mAh/g)	Capacity retention (%-13th)
300	3.57	55.0	0.51	3.63	20.4	83.9	96.7
400	3.74	56.1	0.53	3.53	26.4	107.4	90.1
500	3.67	56.2	0.52	3.52	27.0	116.9	88.7
600	3.74	56.3	0.53	3.51	27.6	108.1	88.4
700	3.70	56.8	0.52	3.49	29.0	82.0	87.0
800	3.73	57.0	0.52	3.43	32.5	82.6	81.4

[a] Measurement by chemical analyses.
[b] Calculated from the concentration and average valence of Mn.

of acetate-derived $LiMn_2O_4$ was much higher than that using sources other than acetate due to the impurity phase of Mn_2O_3 and Li_2MnO_3. In order to further understand the effect of calcination temperature on behavior of single-phase $LiMn_2O_4$, the chemical analysis and charge–discharge cycling were conducted to investigate the chemical composition, capacity, and capacity retention of single-phase $LiMn_2O_4$. Table 1 shows the chemical analyses and electrochemical properties of single-phase $LiMn_2O_4$ calcined at various temperatures. The valence of manganese ions was determined using titration method. It is known that $LiMn_2O_4$ processed at higher temperatures exhibits lower average valences (21). The result in Table 1 also shows the same trend although this result shows average oxidation state of Mn less than 0.35. The reason may be due to large amount of tartrate compounds in the precursor which lower the oxygen partial pressure during the synthesis of $LiMn_2O_4$. The average valence of manganese decreased from 3.63 to 3.43 with calcination temperature increasing from 300 to 800°C. The samples calcined at 300°C having higher average valence of manganese of 3.63 exhibit low initial capacity. During charge process, the Mn^{3+} must release one electron and be oxidized to Mn^{4+}. Lithium manganese oxide with Mn valence greater than 3.5 will have less Mn^{3+} ions for discharge reaction. On the other hand, sample calcined at 500°C shows an initial capacity of 117 mAh/g due to manganese valence close to 3.5. For the sample calcined at temperatures greater than 700°C, it shows low average valence of manganese and low initial capacity because the average valence of manganese is far below 3.5. Under this circumstance. $LiMn_2O_4$ tends to transforms from cubic to tetragonal structure due to the well-known Jahn–Teller distortion (20, 22–24).

In addition, the capacity after cycling test is also dependent on the average valence of manganese. After 13 cycles, the remaining capacity decreased from 96.7 to 81.4% when concentration of Mn^{3+} increased from 20.4 to 32.5%. It is well known that the Mn^{3+} in the high spin state (one d electron in an e_g orbital) will induce the Jahn–Teller distortion (25). The Jahn–Teller distortion reduces the symmetry of the spinel from cubic to tetragonal ($c/a = 1.16$). It also causes the electrode to fracture at the particle surface (19). This effect destroys structural integrity and particle–particle contacts, which are essential for maintaining the electronic conductivity of the electrode.

4. CONCLUSION

Single-phase $LiMn_2O_4$ spinel was synthesized by tartaric acid gel process using lithium acetate and manganese acetate as sources. The Mn_2O_3 and Li_2MnO_3 impurity phases with nonstoichiometric $Li_{1-2z}Mn_{2-2y-z}O_{4-3y-3z}$ were obtained when lithium nitrate and/or manganese nitrate were used as sources. Lithium ion from lithium acetate salt bonds strongly with O–H stretching and carboxylate anion of tartaric acid, but the lithium ion from lithium nitrate salt bonds only with O–H stretching. The first discharge capacity of single-phase stoichiometric $LiMn_2O_4$ powders synthesized at 500°C delivered 117 mAh/g, which was higher than that of $Li_{1-2z}Mn_{2-2y-z}O_{4-3y-3z}$ with an impurity phase of Mn_2O_3 and Li_2MnO_3 derived from nitrate salts. The cycling capacity for single-phase $LiMn_2O_4$ decreased with increasing concentration of Jahn–Teller ion, Mn^{3+}.

ACKNOWLEDGMENT

This work was financially supported by the National Science Council of Taiwan, Grant NSC 88-2216-E-006-052, which is gratefully acknowledged.

REFERENCE

1. D. Guyomard and J. M. Tarascon, *J. Electrochem. Soc.* **139,** 937–948 (1992).
2. G. X. Wang, D. H. Bradhurst, H. K. Liu, and S. X. Dou, *Solid State Ionics* **120,** 95–101 (1999).
3. A. Manthiram, *JOM* **49,** 43–46 (1997).
4. Y. Gao and J. R. Dahn, *J. Electrochem. Soc.* **143,** 100–114 (1996).
5. J. M. Tarascon, M. R. McKinnon, T. N. Bowmer, G. Amatucci, and D. Guyomard, *J. Electrochem. Soc.* **141,** 1421–1431 (1994).

6. J. M. Tarascon and D. Guyomard, *Electrochim. Acta* **38,** 1221–1231 (1993).
7. S. R. S. Prabaharan and C. Julien, *Solid State Ionics* **112,** 25–34 (1998).
8. S. Passerini, F. Coustier, M. Giorgetti, and W. H. Smyrl, *Electrochem. Solid-State Lett*. **2,** 483–485 (1999).
9. W. Yang, Q. Liu, W. Qiu, S. Lu, and L. Yang, *Solid State Ionics* **121,** 79–84 (1999).
10. Y. Xia, H. Takeshige, H. Noguchi, and M. Yoshio, *J. Power Sources* **56,** 61–67 (1995).
11. Y. M. Hon, H. Y. Chung, K. Z. Fung, and M. H. Hon, *J. Solid State Chem.* **160,** 368–376 (2001).
12. Y. M. Hon, K. Z. Fung, and M. H. Hon, *J. Ceram. Soc. Jpn.* **108,** 462–468 (2000).
13. Y. M. Hon, K. Z. Fung, and M. H. Hon, *J. Euro. Ceram. Soc.* **21,** 515–522 (2001).
14. W. Liu, G. C. Farrington, F. Chaput, and B. Dunn, *J. Electrochem. Soc.* **143,** 879–884 (1996).
15. S. P. Lin, K. Z. Fung, Y. M. Hon, and M. H. Hon, *J. Crystal Growth*, **226,** 148–157 (2001).
16. S. Choi and A. Manthiram, *J. Electrochem. Soc.* **147,** 1623 (2000).
17. A. Momchilov and A. Kozawa, *J. Power Sources* **41,** 305–314 (1993).
18. P. Barboux and F. K. Shokoohi, *J. Solid State Chem.* **94,** 185–196 (1991).
19. Y. M. Hon, S. P. Lin, K. Z. Fung, and M. H. Hon, *J. Euro. Ceram. Soc.* in press (2001).
20. Y. K. Sun, K. H. Lee, S. I. Moon, and I. H. Oh, *Solid State Ionics* **112,** 237–243 (1998).
21. J. Sugiyama, T. Hioki, S. Noda, T. Atsumi, and N. Kamegashira, *J. Alloys Compounds* **235,** 163–169 (1996).
22. W. Liu and G. C. Farrington, *J. Electrochem. Soc.* **143,** 3590–3596 (1996).
23. F. Shinshu and Y. Nitta, *J. Power Sources* **68,** 609–612 (1997).
24. Y. S. Horn and W. F. Howard, *J. Electrochem. Soc.* **145,** 16–23 (1998).
25. A. Yamada, K. Miura, K. Hinokuma, and M. Tanaka, *J. Electrochem. Soc.* **142,** 2149–2156 (1995).